Limits and Opportunities for Miniaturizing Ultrasonic Surgical Devices Based on a Langevin Transducer

Xuan Li, Thomas Stritch, Kevin Manley, and Margaret Lucas, *Member, IEEE*

***Abstract*— Minimally invasive surgery offers opportunities for reduced morbidities, faster postoperative recovery, and reduced costs, and is a major focus of surgical device innovation. For ultrasonic surgical devices, which offer benefits of high precision, low force, and tissue selectivity in surgical procedures, there exist laparoscopic ultrasonic shears for minimally invasive surgeries that combine tissue cutting with vessel hemostasis and sealing functions. Another approach to laparoscopy that could enable new procedures, and increase the sites of surgeries that could be reached by an ultrasonic device, involves integrating a miniature ultrasonic tool with a flexible surgical robot. However, miniaturization presents challenges in delivering the ultrasonic vibrational energy required to cut hard and soft tissues, partly due to the concomitant small volume of piezoelectric material. This article aims to provide insights into the trade-offs between transducer size, volume of piezoceramic material, resonance frequency, and the achievable displacement amplitude of devices that, consistent with current ultrasonic surgical tools, are based on a bolted Langevin transducer (BLT) and tip. Different configurations of BLTs are studied, including a cascaded version, simple bar versions, and BLTs with different front mass geometries. Results show that a BLT with a larger number of piezoceramic rings exhibits a higher coupling coefficient k_{eff} but with the compromise of a lower mechanical Q and stronger nonlinear response at increasing excitation levels. Displacement amplitude is reduced considerably when a BLT is excited at a higher harmonic, where the PZT rings are maintained at a nodal plane, and the resonance frequency shift at increasing excitation levels increases significantly. The electromechanical and dynamic characteristics of a cascaded transducer excited in its third longitudinal mode (L3) are almost equivalent to a much shorter version of a BLT driven at the same frequency but in its first longitudinal mode (L1), showing that a cascaded BLT can be a realistic proxy for studying the dynamics of small BLT devices. A new figure of merit is proposed that is the product of Q, k_{eff}^2, and gain, which accounts for the gain of cylindrical BLTs which is shown not to be unity. It also proves effective as it incorporates the key factors affecting the achievable displacement amplitude of a BLT, including for BLTs with gain profiles in the front mass. The order of highest to lowest amplitude of a series of six gain-profile BLTs matches the order estimated by the figure of merit. It is shown that a BLT with a stepped profile front mass can achieve displacement that has the potential to cut hard or soft tissue and exhibits the smallest shifts in resonance frequency at increasing excitation levels.**

***Index Terms*— Langevin transducer, miniaturization, minimally invasive surgery, ultrasonic surgical device.**

I. Introduction

ULTRASONIC surgical devices generally operate in resonance at an ultrasonic frequency in the 20–70 kHz range and have proven to provide precise tissue cutting with low lateral mechanical and thermal damage and effective hemostasis [1].

For cutting of hard tissue, where the devices operate at the lower ultrasonic frequencies (generally between 20 and 35 kHz), surgical tips exhibit tissue selectivity [2] and require low cutting force due to the inherent characteristics of the ultrasonic cutting and fragmentation mechanisms. The first ultrasonic devices for bone cutting can be dated back to the early 1950s, for applications in dentistry [3], although commercial devices for osteotomies only emerged 50 years later [4]. Originally adopted for oral and maxillofacial surgical procedures, the technology is now more widely used in neuro and spinal surgeries and orthopedics [5]–[9].

For soft tissue cutting that performs both dissection and vessel sealing, larger ultrasonic amplitude and higher frequency (normally above 50 kHz) are commonly used [10], [11]. It has been reported that although the operating resonance frequency has little effect on the soft tissue coagulation depth, the higher resonance frequency increases the tissue coagulation ratio (defined as the ratio of area of coagulated region to surface area of the tip) significantly [12]. These devices, often referred to as ultrasonic shears, have also adopted for laparoscopic surgeries [13].

Although there have been numerous innovations and performance advancements of ultrasonic surgical device technology since its emergence, including different geometries of surgical tips for specific procedures [14], [15], different surgical tip vibration modes [16]–[18], and particularly advances in

Manuscript received November 28, 2020; accepted March 7, 2021. Date of publication March 10, 2021; date of current version June 29, 2021. This work was supported in part by the EPSRC Impact Acceleration Account with co-funding by Stryker under Grant EP/R511705/1 and in part by EPSRC the Program Grant (Ultrasurge–Surgery enabled by Ultrasonics) under Grant EP/R045291/1. *(Corresponding author: Margaret Lucas.)*

Xuan Li and Margaret Lucas are with the Centre for Medical and Industrial Ultrasonics, James Watt School of Engineering, University of Glasgow, Glasgow G12 8QQ, U.K. (e-mail: margaret.lucas@glasgow.ac.uk).

Thomas Stritch and Kevin Manley are with Stryker Instruments, Cork, T45 HX08 Ireland.

Digital Object Identifier 10.1109/TUFFC.2021.3065207

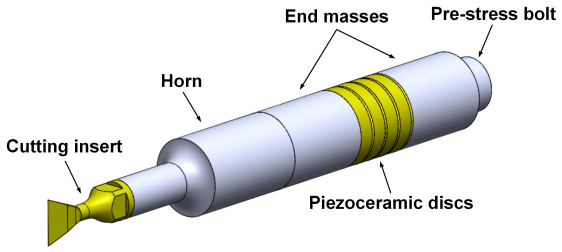

Fig. 1. Structure of a typical ultrasonic device.

drive electronics [19], the consistent configuration of a tuned Langevin-style transducer [bolted Langevin transducer (BLT)] with a resonance horn (or waveguide) and tip insert has remained unchanged.

Fig. 1 shows the basic structure of a BLT-based device. Commercial devices will typically accommodate a series of interchangeable cutting inserts whose geometries are procedure specific. The device shown comprises a BLT with a stack of piezoceramic rings sandwiched, using a prestress bolt, between two end masses, plus a horn with a tapered or stepped profile to amplify the oscillation displacement amplitudes generated from the piezoceramic rings to the cutting tip. In this example, the device is one full wavelength of the tuned longitudinal-mode frequency; the BLT is a half-wavelength and the horn and cutting tip combination is a half-wavelength. The whole ultrasonic device could alternatively be a half-wavelength by integrating the horn and tip into the front mass to create a shorter device, or a larger multiple of a half-wavelength, for example, to create a laparascopic device. However, the generic BLT configuration, which limits the geometrical design envelope to device lengths of multiples of a half wavelength of the longitudinal-mode frequency, poses challenges for device miniaturization.

The straightforward solution for creating a smaller length device is to operate at a higher resonance frequency, which is not consistent with the low ultrasonic frequencies currently used in commercial bone cutting devices. Also, a smaller diameter device means less space for the volume of piezoelectric material that is generally needed for tissue cutting. Some alternative solutions have been proposed, including incorporating ultrasonic vibration actuation in a flextensional transducer [20]. To date, these have been lab-based prototypes and, although the results demonstrate that bone cutting is possible in devices considerably smaller in length than current BLT devices, the width (or diameter) dimension has tended to be larger in order to accommodate sufficient piezoelectric material.

The advantage of miniature devices, with both small length and small diameter, is the capability they offer for minimally invasive surgeries. Future innovations can, for example, be enabled through miniature devices that deliver the ultrasonic energy directly at the site of surgery through a small access route, or by integrating small ultrasonic surgical devices with flexible robotics, where the device can be maneuvered and navigated to more difficult to reach surgical sites along tortuous pathways through small access routes [21]–[23]. To evaluate potential solutions for small devices, the devices used here have a diameter of 8 mm and length in the 50–70 mm range. The target peak–peak displacement is at least 30 μm, which is at the lower end of ultrasonic displacements used to cut hard and soft tissues. We have set this amplitude requirement to be at least 30-μm peak-to-peak in this study, to be consistent with the lowest amplitude settings of a number of current ultrasonic hard and soft tissue cutting devices [11], [20], [24]–[27]. Here, we investigate the factors that both limit and assist miniaturization of devices are based on a resonance longitudinal-mode BLT configured with a gain-horn and tip.

TABLE I
DEVICE NOMENCLATURES

PHOTO OF BLTS	NAME
	$BLT_{(2)}^{(Control)}$
	$BLT_{(4)}^{(Control)}$
	$BLT_{(6)}^{(Control)}$
	$BLT_{(4-4-4)}^{(Cascaded)}$
	$BLT_{(4)}^{(Bar)}$
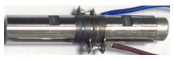	$BLT_{(4)}^{(Cylindrical)}$
	$BLT_{(4)}^{(Stepped)}$
	$BLT_{(4)}^{(Catenoidal)}$
	$BLT_{(4)}^{(Exponential)}$
	$BLT_{(4)}^{(Conical)}$
	$BLT_{(4)}^{(Cosine)}$

II. METHODOLOGY

A range of different BLTs is studied to elicit the knowledge of associated dynamic responses and how they benefit or limit miniaturization. These BLTs are all presented in Table I. The nomenclature is BLT with a superscript that either identifies the control devices or indicates the distinguishing shape of the front mass and a subscript that indicates the number or arrangement of the identical PZT elements. It should be noted that the small filet introduced at the diameter reduction of the stepped profile front mass is to reduce stress at that location but does not affect the gain.

The investigation begins with a study of three slender bars, which form a single set of BLTs with an increasing number of piezoceramic elements. These bars are all nominally a half wavelength at 20 kHz, therefore tuned to the first longitudinal mode (L1), but they can also be excited at higher harmonics.

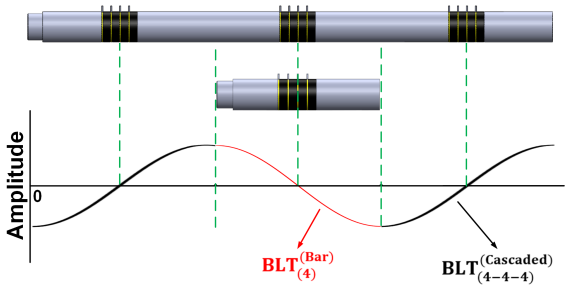

Fig. 2. $BLT^{(Cascaded)}_{\triangleright 4\text{-}4\text{-}4 \triangleleft}$ and $BLT^{(Bar)}_{(4)}$ and the longitudinal waveform.

The three bars act as a set of simple control BLTs (see Table I) tuned to a low ultrasonic frequency typical of power ultrasonic devices, and against which the ultrasonic vibrational response and behaviors of smaller devices can be compared.

Next, a cascaded BLT is introduced, Fig. 2, consisting of three sets of piezoceramic rings that are connected mechanically in series and electrically in parallel, and are sandwiched by four metal masses. This configuration is tuned to its third longitudinal mode (L3) frequency at around 60 kHz, and all three sets of piezoceramic rings are centered on nodal planes in this mode. This cascaded BLT is studied in order to compare its dynamic responses in L3 mode with that of a much shorter BLT with a single set of PZT rings that is tuned to L1 mode at around 60 kHz [$BLT_{(4)}{}^{(Bar)}$ in Table I]. The question posed here is: does the cascaded transducer excited in L3 mode behave dynamically similar to a BLT excited in L1 mode that is roughly a third of the length (see Fig. 2). This is an important insight for understanding the dynamics of short L1-tuned devices and how the achievable ultrasonic amplitude of a BLT is affected by size. In addition, the response of the cascaded BLT is compared to one of the control BLTs [$BLT^{(Control)}_{(4)}$ in Table I] excited in L3 mode, to study the effect of the volume of the PZT on the dynamic performance. Finally, six small BLTs are studied, with dimensions of approximately 8 mm in base diameter, 2.5 mm for the tip diameter, and 50–70 mm in length and with different geometries of tapered front mass. The aim is to characterize the amplitude of amplification gains and dynamic response of the six configurations and identify how these, as well as the electromechanical coupling and mechanical Q, are affected by the size of the BLT and the shape of the front mass.

A hard PZT piezoceramic (PIC-181, PI Ceramic) material is used for all BLTs, with all piezoceramic rings acquired from a single batch supply to ensure consistency of properties. The dimensions and piezoelectric material properties are presented in Table II. The metal masses in the BLTs are titanium grade 5 alloy, Ti-6Al4V, the prestress bolt is A2 tool steel, and the electrode material is copper, with material properties listed in Table III.

III. BLT Design and Characterization

A. Design of BLTs

The initial study compares the vibration response of 8-mm-diameter cylindrical BLTs tuned to L1 at around 20 kHz. The BLTs have one, two, and three pairs of piezoceramic rings, and are modeled and tuned using finite-element analysis (FEA)

TABLE II
PIC-181 PZT Material Properties

Outer diameter [mm]	8
Inner diameter [mm]	4.3
Thickness [mm]	2
Density ρ [kg/m^3]	7800
Relative permittivity ε^T_{11}	1500
Relative permittivity ε^T_{33}	1200
Piezoelectric charge coefficient d_{31} [pC/N]	−120
Piezoelectric charge coefficient d_{33} [pC/N]	265
Piezoelectric charge coefficient d_{15} [pC/N]	475
Elastic compliance coefficient S^E_{11} [m^2/N]	1.18×10^{-11}
Elastic compliance coefficient S^E_{33} [m^2/N]	1.42×10^{-11}
Mechanical quality factor Q	2000

TABLE III
Transducer Metals Material Properties

Material	Ti6Al4V	A2 Tool Steel	Copper
Density [kg/m^3]	4430	7860	8900
Young's Modulus [GPa]	109	203	110
Poisson's Ratio	0.313	0.285	0.370
Acoustic Impedance [Pa · s/m × 10^6]	27.32	45.40	41.61

software package (Abaqus-Simulia, Dassault Systèmes). If the BLT is excited at an odd longitudinal-mode (L1, L3, L5...), the piezoceramic elements are located at the nodal plane, and hence are resonance tuned [28]. The even number modes are not considered in this study because piezoceramic rings are located at antinodal planes, antiresonance tuned, which generally results in a low effective coupling coefficient, k_{eff}, and a low oscillation amplitude [29].

Six amplitude gain profiles are introduced into the BLT front mass to increase the vibration amplitude. The relative effectiveness of these classical gain-horn profiles on smaller devices is investigated by comparing with theoretical calculation and published results on larger (20 kHz) devices. The profiles are cylindrical, catenoidal, conical, cosine, exponential, and stepped.

The short devices consist of four piezoceramic rings and their length ranges from 50 to 70 mm, depending on the horn geometry. During assembly, the transducer components were prestressed following guidelines for achieving a stable response without risking depolarisation [30], [31]. For an applied prestress in the recommended region of less than 30 MPa [32], the applied torque is determined to be not more than 3.0 N · m. For each BLT, the correct pre-stress was identified by monitoring the impedance–frequency characteristics as the applied torque was increased. The resonance and antiresonance frequencies increased but then stabilized when the required prestress was reached.

B. Characterization

The BLTs were all characterized using electrical impedance analysis (IA), experimental modal analysis (EMA), and harmonic response analysis.

1) Electrical Impedance Analysis: IA measurements are performed using an impedance analyzer (Agilent 4395A). A swept signal of 1-V peak-to-peak over a bandwidth covering the frequency range of interest was applied, and the impedance

spectrum was measured. The effective electromechanical coupling coefficient, k_{eff}, was calculated from the impedance spectrum data using the following equation [33], providing a measure of the BLT conversion efficiency from electrical energy to mechanical vibrations:

$$k_{\text{eff}}^2 = \frac{f_a^2 - f_r^2}{f_a^2} \tag{1}$$

where f_a is the antiresonance frequency and f_r is the resonance frequency.

Mechanical Q is also considered here because it is an important indicator of a power ultrasonic device's potential to achieve high ultrasonic amplitudes and low losses. However, Q of PZT material tends to exhibit an inverse relationship with k_{eff} [34]. Therefore, for BLTs there is a trade-off between the volume of PZT and the size of the transducer in trying to simultaneously increase k_{eff} while maintaining a high Q, and hence maximize the power of the device [35].

2) Experimental Modal Analysis: EMA is performed by measuring the frequency response functions (FRFs) from a grid of vibration response measurement points on the transducer surface, from which the modal parameters (frequency, damping, and mode shape) are extracted [36]. A white noise excitation signal of 15 V_{rms} is generated by a signal generator (Quattro, Data Physics) and amplified by a power amplifier (QSC RMX 4050HD), before being supplied to the transducers. A 3-D laser Doppler vibrometer (CLV3000, Polytec) is used to measure three orthogonal components of the vibrational velocities from the grid points. Data acquisition and processing software (SignalCalc, Data Physics) is used to calculate the FRFs from the excitation and response signals and then to apply curve-fitting routines to extract the magnitude and phase data. Finally, the measured FRFs are exported to modal analysis software (ME'scopeVES, Vibrant Technology, Inc., Centennial, CO, USA) to extract modal parameters.

3) Harmonic Response Analysis: To study the vibration responses of the BLTs excited in resonance at higher excitation levels, harmonic analysis experiments are performed. A BLT is excited via a frequency sweep through a range from below to above the resonance, using a burst sine signal generated from a signal generator (Agilent 33210A) and amplified by a power amplifier (HFVA-62). The longitudinal vibration response is measured using a 1-D laser Doppler vibrometer (OFV 303, Polytec, Polytec GmbH, Waldbronn, Germany) from a grid point on the BLT front face.

To minimize frequency shifts due to thermal effects of the PZT elements at high excitation levels, each sine burst signal has a fixed 6000 oscillation cycles, which is sufficient to ensure steady state is reached, but is sufficiently short to minimize heating. Furthermore, a 3.0-s time interval between sequential bursts ensures a constant temperature is maintained for the complete frequency sweep. Response data are captured with a resolution of 5 Hz, which is sufficiently small to observe detailed changes in the vibration response. The excitation voltage is stepped from 1, then 10 to 100 V (rms) in increments of 10 V and the displacement amplitude–frequency response is measured at each excitation level.

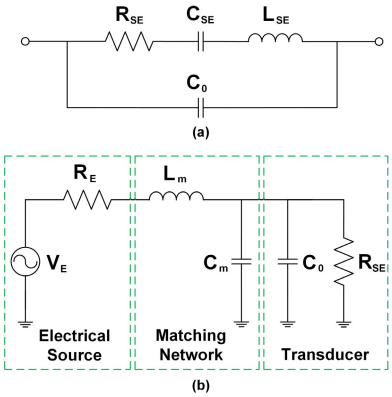

Fig. 3. (a) BVD model at resonance and (b) simplified equivalent circuit at resonance with an *LC* matching network configuration.

C. Impedance Matching

To optimize the energy transmission efficiency of the BLTs, it is crucial to match the output impedance of the signal generator and power amplifier, which is normally 50 Ω, to the impedance of the ultrasonic transducer. A matching circuit is designed by modeling the transducer as an electrical circuit at its resonance.

There are a number of equivalent electrical circuit models which can be used to represent a transducer at the series resonance, and the most common being the Butterworth–Van Dyke (BVD) model [37], shown in Fig. 3(a). R_{SE} represents the radiation and mechanical losses of the transducer. The motion capacitance and inductance, C_{SE} and L_{SE} respectively, model the resonance performance of the transducer, and C_0 is the clamping capacitance of the transducer. The impedance of the BVD model can then be calculated from the following equation:

$$Z(\omega) = \frac{1}{\omega C_0}\left(\frac{\left(\omega_{\text{s}}^2 - \omega^2\right) + \text{j}\omega\frac{R_{\text{SE}}}{L_{\text{SE}}}}{-\omega\frac{R_{\text{SE}}}{L_{\text{SE}}} + j\left(\omega_{\text{p}}^2 - \omega^2\right)}\right) \tag{2}$$

where ω_{s} and ω_{p} are the series and parallel angular resonance frequencies, respectively, calculated from the following equation:

$$\omega_{\text{s}} = \sqrt{\left(\frac{1}{L_{\text{SE}}C_{\text{SE}}}\right)}$$
$$\omega_{\text{p}} = \sqrt{\left(\frac{C_{\text{SE}} + C_0}{L_{\text{SE}}C_{\text{SE}}C_0}\right)}. \tag{3}$$

At series resonance, the combined effect of the reactive components, L_{SE} and C_{SE}, exhibits a phase of 0°. The transducer presents a purely resistive characteristic, and the circuit simplifies to R_{SE} in parallel with C_0.

Fig. 3(b) shows the simplified equivalent circuit of a transducer excited by an electrical source through an *LC* configured matching network. V_{E} is the electrical source, R_{E} is the resistance of the source which is around 50 Ω, and L_{m} and C_{m} are the inductance and capacitance of the matching network respectively, which can be calculated from the following

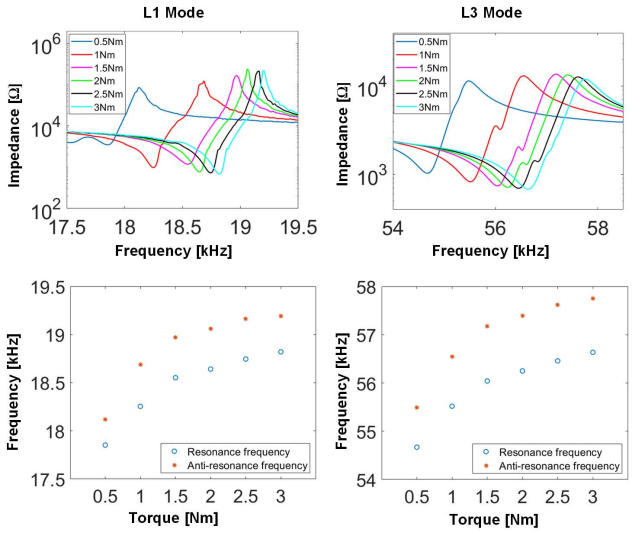

Fig. 4. Impedance–frequency spectrum measurements of the L1 and L3 modes showing the change of resonance and antiresonance frequencies of $\mathrm{BLT}_{(4)}^{(\mathrm{Control})}$.

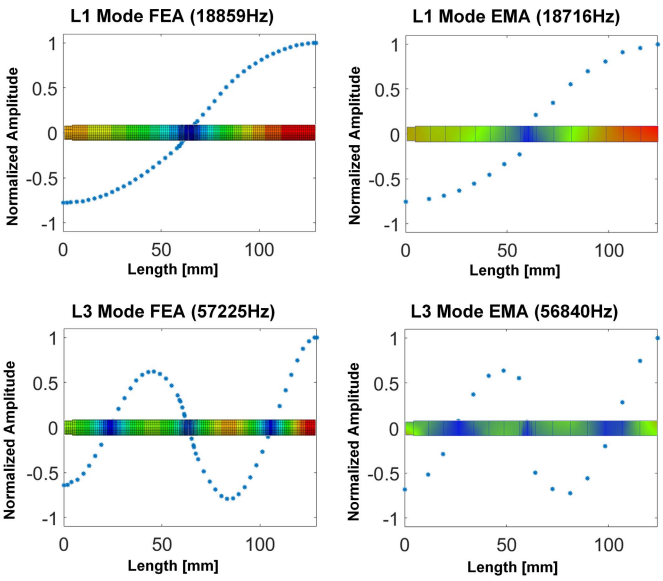

Fig. 5. FEA predicted and EMA measured normalized L1 and L3 mode waveforms of $\mathrm{BLT}_{(4)}^{(\mathrm{Control})}$.

equation [37]:

$$L_{\mathrm{m}} = \frac{R_{\mathrm{E}}}{\omega}\sqrt{\left(\frac{R_{\mathrm{SE}}}{R_{\mathrm{E}}} - 1\right)}$$
$$C_{\mathrm{m}} = \frac{1}{\omega R_{\mathrm{SE}}}\sqrt{\left(\frac{R_{\mathrm{SE}}}{R_{\mathrm{E}}} - 1\right)} - C_0. \tag{4}$$

The impedance and resonance frequency of the BLTs in this study are measured using the impedance analyzer, and the parameters of the BVD model R_{SE}, C_{SE}, L_{SE}, and C_0 are also extracted from these measurements. The LC matching network is implemented by selecting a capacitor, of capacitance as calculated in (4), and the inductor is fabricated by winding a 1-mm-diameter copper wire around a toroidal ferrite core. The number of turns of the winding is adjusted until the highest level of vibration amplitude at the BLT end face is reached.

IV. Results

A. Results of the Control BLTs

Fig. 4 shows the measured impedance of $\mathrm{BLT}_{(4)}^{(\mathrm{Control})}$ for the L1 and L3 modes, illustrating the identification of the required torque applied to the bolt to achieve a sufficient pre-stress for electrical stability of the transducer. As can be seen in Fig. 4, the change in the resonance frequency diminishes as the torque is increased. When no further resonance frequency change is measured, electrical stability has been reached. For the BLTs shown here, at a torque of 3 N·m there was no further increase in the resonance or antiresonance frequencies.

The electromechanical coupling coefficient k_{eff}, which is an important figure of merit to evaluate the ratio of delivered mechanical energy to the stored total energy in the transducer, is calculated from the resonance and anti-resonance frequencies. Additionally, the Q factor is calculated from the impedance at series resonance, which indicates the amount of converted mechanical energy preserved in the transducer, with a higher Q value offering a narrower bandwidth and a lower damping.

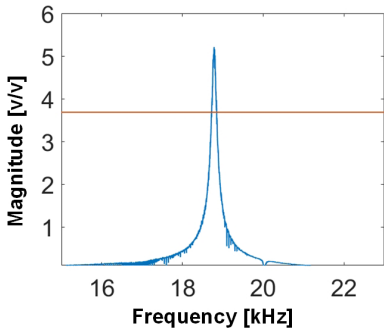

Fig. 6. Example of the FRF measurement of $\mathrm{BLT}_{(4)}^{(\mathrm{Control})}$ at L1 mode.

However, high Q can also result in more challenging control under load fluctuation [35]. Importantly for power ultrasonic devices, both coupling coefficient k_{eff} and Q are calculated here from a static and low excitation IA, which may not be constant or representative of high dynamic excitation levels.

The mode shapes and modal frequencies (Fig. 5) are in close agreement between FEA predictions and EMA measurements, including the precise locations of the nodal and antinodal planes. An important observation is that the cylindrical bar presents a nonunity gain for both L1 and L3 modes, as calculated from the normalized amplitude at the end of the front mass and back mass. For these BLTs, this is due to the uneven mass distribution of the prestress bolt, which requires the front mass to be a little longer than the back mass to locate the PZT rings centered on the nodal plane.

The damping ratio of the transducer is extracted from averaged FRF measurements from the bandwidth at -3 dB of the peak response. Fig. 6 shows an example of the averaged FRF, where the red line is at -3 dB. From this, mechanical Q is calculated for all BLTs under dynamic excitation, which should be more representative of the operating conditions of the BLTs.

The vibration responses of the three control BLTs with impedance matching networks are presented in Fig. 7. The

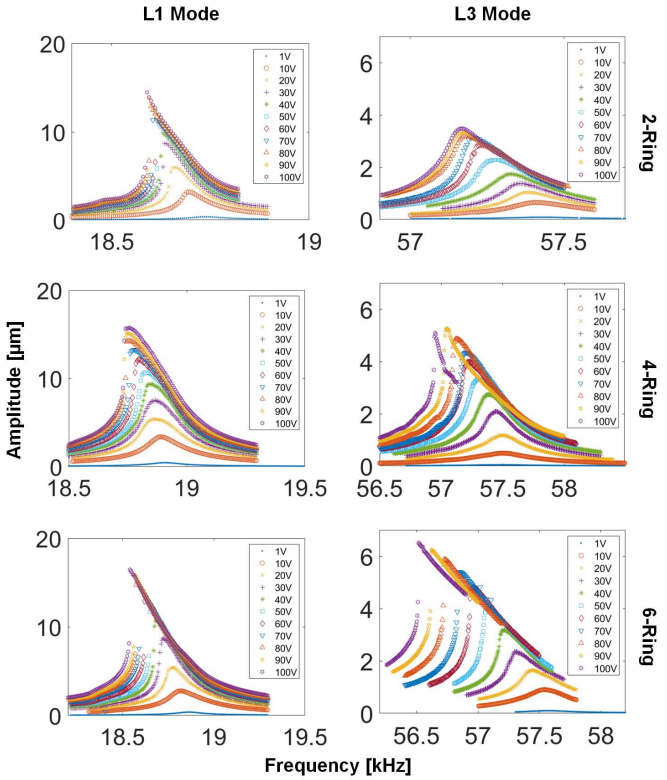

Fig. 7. Vibration response from harmonic response analysis of the three control BLTs for L1 and L3 modes.

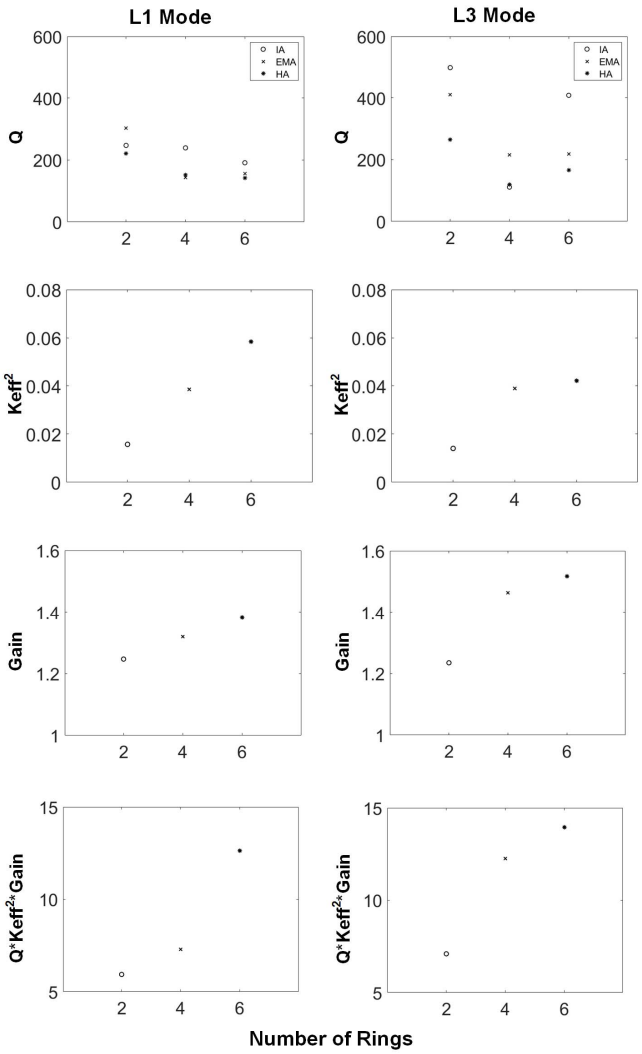

Fig. 8. Q, k^2_{eff}, gain, and the product ($Q \times k^2_{\text{eff}} \times$ gain) for L1 and L3 modes for the three control BLTs ratio combined with the higher losses associated with additional interacting surfaces.

first observation is that the ultrasonic amplitude of the control BLTs in L1 mode is much higher than L3 mode for the same excitation level, reaching over 15 and 6 μm for $\text{BLT}^{(\text{Control})}_{(6)}$ at 100 V (rms), due to lower energy in higher harmonics. For both modes, the ultrasonic amplitude increases with number of PZT rings. A softening nonlinear response is observed for all configurations and excitation levels, exhibited in Fig. 7 as a series of response curves whose backbone bends toward the left [38]. Mechanical Q is also calculated from these measurements, from the response at the lowest excitation of 1 V that presents the most linear (symmetric) response curve around the resonance.

In order to interrogate these vibration responses, presented in Fig. 8, are the Q values calculated from the three different measurements (IA, EMA, and HA), and also the square of the coupling coefficient, as k^2_{eff}, the amplitude gain and the product of Q, k^2_{eff}, and gain (using the Q values extracted from EMA).

The Q values show a significant spread between different measurement data from which they are calculated, indicating a change in the capability of the transducer to preserve the converted mechanical energy as the driving condition changes. Q values extracted from the harmonic response analysis measurements at 1-V excitation, from EMA measurements at 15-V excitation and from IA, show how losses in these BLTs under excitation conditions are not well captured by IA and that Q is not constant at different excitation levels. From both dynamic measurements, Q decreases for both modes from two to four PZT rings, from 300 to 150 for L1 and 500 to 100 for L3, and there is little change from four to six rings. This is consistent with a lower Q for BLTs with a higher PZT to metal

There is a linear relationship between k^2_{eff} and number of PZT rings. However, this trend is known to saturate when the PZT rings cover half of the BLT equivalent length, where equivalent length is the full length of the transducer in the L1 mode [35]. This saturation can be seen for the 6 PZT ring BLT in the L3 mode, where the equivalent length is now a third of the length of the transducer. This trend is also exhibited in the gain, with a linear increase with number of rings in L1 mode and a saturation in gain in the L3 mode.

The combined effect of $Q \times k^2_{\text{eff}}$ has been considered previously as a figure of merit in maximizing transducer performance [35]. However, it is clear from Fig. 8 that the measurement of Q is not consistent between measurement methods and that the gain of a BLT cannot be assumed to be an unity. It is therefore proposed that the product of Q, k^2_{eff}, and gain, where Q is extracted from EMA, will be a more suitable figure of merit for power ultrasonic devices where the aim is to excite high ultrasonic amplitude. The results show an increase with number of PZT rings in the transducer for the BLT in both modes, and are consistent with the displacement amplitudes in Fig. 7 for all three control devices.

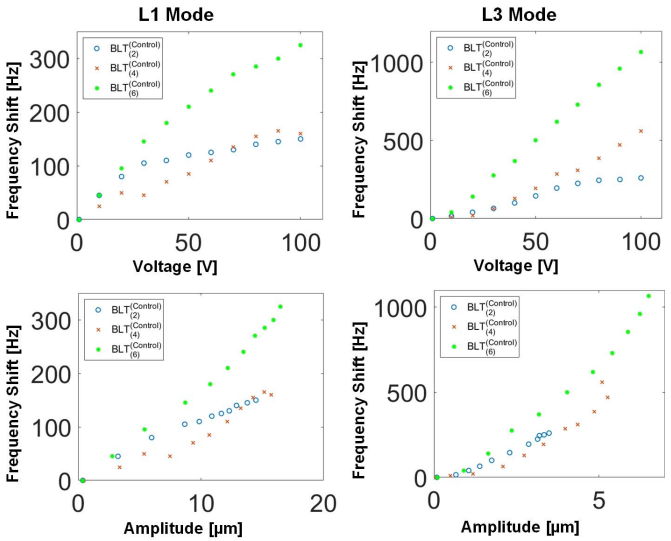

Fig. 9. Resonance frequency shift of control BLTs in L1 and L3 modes at increasing excitation level and displacement amplitude.

Fig. 9 shows how the change in the resonance frequency, as defined by the change from the resonance frequency at 1-V excitation, increases with increased applied voltage (excitation level) and with increasing displacement amplitude in L1 and L3 modes for all the control BLTs, using data from Fig. 7. As the effects of temperature have been eliminated from these measurements, frequency shifts are mainly due to nonlinearity in piezoelectric properties at higher excitation levels, which can cause loss of performance and efficiency in ultrasonic transducers [39]. The BLT with six PZT rings has the lowest Q (see Fig. 8) due to its high PZT to metal ratio and largest number of interfaces. It also exhibits very large frequency shifts because of this high volume of PZT and because it achieves a higher amplitude, or a larger material strain. Frequency shifts up to 300 Hz and 1 kHz were measured in L1 and L3 modes, respectively.

These results for the control BLTs provide some expectations for the challenges of creating small BLTs. Where the resonance frequency is similar to the L3 mode frequency of the control BLTs, and a larger PZT to metal ratio is needed to achieve sufficient ultrasonic amplitude to cut hard or soft tissues, the frequency shifts at high excitation levels could make resonance control and tracking very difficult and jeopardize the stability of the device.

B. Cascaded Transducer

The cascaded BLT with three sets of four PZT rings in L3 mode is compared with both the control BLT with four rings in L3 mode and the BLT with four rings that is approximately one third of its length in L1 mode. These transducers are presented in Table I as $\mathrm{BLT}_{(4-4-4)}^{(\mathrm{Cascaded})}$, $\mathrm{BLT}_{(4)}{}^{(\mathrm{Control})}$, and $\mathrm{BLT}_{(4)}{}^{(\mathrm{Bar})}$. The impedance measurements are presented in Fig. 10.

The cascaded BLT in L3 mode has a very low impedance but a similarly wide bandwidth, $(f_a - f_r)$, as the small BLT in L1 mode, which results in a higher electromechanical coupling coefficient than the control BLT. However, $\mathrm{BLT}_{(4)}{}^{(\mathrm{Control})}$ exhibits a sharper trough at the series resonance

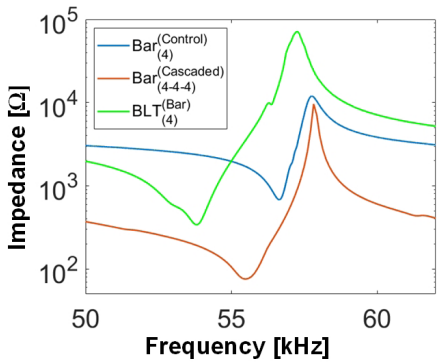

Fig. 10. Measured impedance of $\mathrm{BLT}_{(4)}^{(\mathrm{Control})}$ and $\mathrm{BLT}_{(4-4-4)}^{(\mathrm{Cascaded})}$ in L3 mode and $\mathrm{BLT}_{(4)}^{(\mathrm{Bar})}$ in L1 mode.

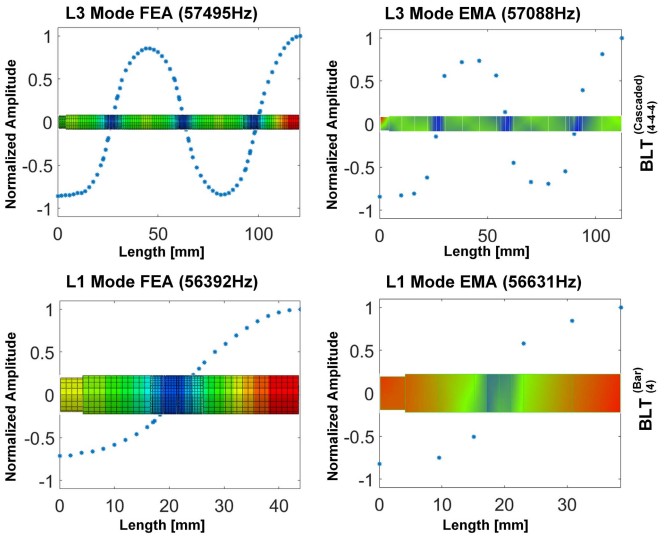

Fig. 11. FEA versus EMA of $\mathrm{BLT}_{(4-4-4)}^{(\mathrm{Cascaded})}$ in L3 mode and $\mathrm{BLT}_{(4)}^{(\mathrm{Bar})}$ in L1 mode.

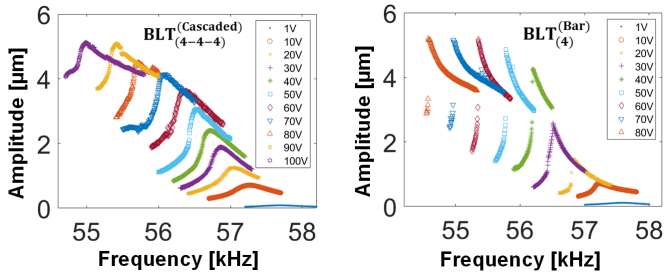

Fig. 12. Harmonic response analysis of $\mathrm{BLT}_{(4-4-4)}^{(\mathrm{Cascaded})}$ in L3 and $\mathrm{BLT}_{(4)}^{(\mathrm{Bar})}$ in L1.

which corresponds to a higher mechanical Q. The impedance of the three BLTs is affected by the ratio of PZT to metal, as was observed in the characterizations of the control BLTs previously. In addition, impedance of $\mathrm{BLT}_{(4)}{}^{(\mathrm{Control})}$ is affected here by having PZT rings at only one of its nodal planes.

The vibration modes and resonance frequencies predicted in FEA and extracted from EMA, as shown in Fig. 11, show a close agreement in the nodal plane locations and gains. Compared with the control BLT in L3 mode (Fig. 5), the cascaded transducer has a slightly lower gain because it has a more even mass distribution.

The vibration response from harmonic response analysis measurements is shown in Fig. 12. For the cascaded BLT,

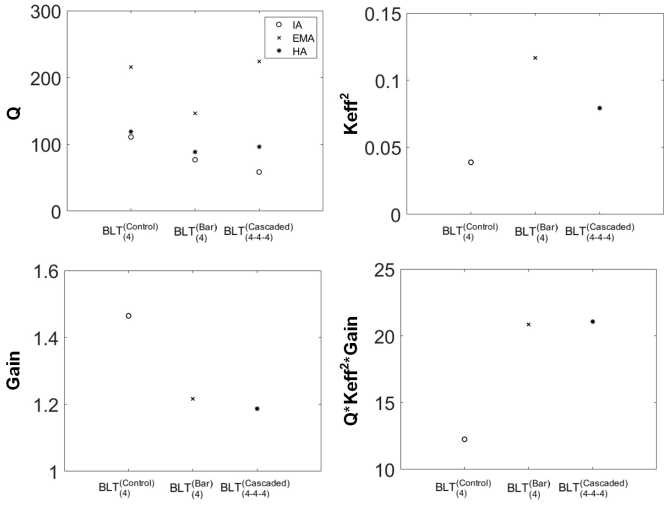

Fig. 13. Q factor, k^2_{eff}, gain, and ($Q \times k^2_{\text{eff}} \times$ gain) for $\text{BLT}^{(\text{Control})}_{(4)}$, $\text{BLT}^{(\text{Bar})}_{(4)}$, and $\text{BLT}^{(\text{Cascaded})}_{(4\text{-}4\text{-}4)}$.

the displacement amplitude ceases to increase beyond 90-V excitation level, which is similar to the control BLT excited in L3 mode shown in Fig. 7. The amplitude saturation of the small

BLT occurs at 60 V, but all three BLTs achieve a very similar amplitude of around 5 μm. This reveals a key limitation of small BLTs to deliver ultrasonic amplitude, but the results also demonstrate how a 20-kHz BLT in L3 (control or cascaded version) is a good predictor of the achievable amplitude of an L1 BLT of approximately a third of its length and three times its fundamental frequency. The cascaded BLT exhibits a similarly wideband impedance response, but the small transducer exhibits a stronger nonlinearity at higher excitation levels.

The data from these results are compared for the three transducers in Fig. 13. Again, the challenge of a realistic measurement of Q is illustrated by the large variations between methods, in this case with the estimations from EMA being around twice the Q values estimated from the IA and 1-V harmonic analysis. The data from EMA are considered to be more representative of the losses under dynamic excitation of the BLTs and this is supported by the results that show the control BLT, which has lower PZT to metal ratio than the small BLT, has the highest Q as the cascaded BLT.

The coupling coefficients further illustrate the impedance measurements that showed a narrow frequency band between the antiresonance and resonance frequencies of the control BLT and a much wider bandwidth of the cascaded and small BLTs, with the small BLT having the highest k^2_{eff} value. Both the gain (of 1.2) and the product ($Q \times k^2_{\text{eff}} \times$ gain) (of 22) of the cascaded and small BLTs are almost equal, again showing how the configuration of the cascaded BLT in L3 mode exhibits very close dynamic characteristics of the small BLT in L1 mode. The use of ($Q \times k^2_{\text{eff}} \times$ gain) as a figure of merit is also supported by clearly distinguishing these two BLTs from the control BLT, which achieves a similar displacement amplitude but is not as close a dynamic model overall for the small BLT as the cascaded configuration.

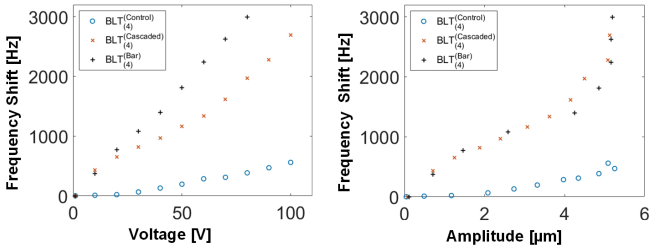

Fig. 14. Resonance frequency shift of the control, cascaded, and small BLTs with increased excitation level and displacement amplitude.

Some caution is necessary for interpreting the results for the design of high power ultrasonic BLTs. It is clear that estimations of Q are very dependent on the measurement methods and therefore on excitation level and these estimations are also affected by the nonlinear response characteristics of the BLTs. The coupling coefficient is calculated from the impedance measurement, and both parameters are unlikely to be constant for increasing excitation levels. This also means that the impedance matching networks, whose inductance and capacitance values are calculated from the IA, may not be an optimal configuration, especially when large shifts in the resonance frequency occur at high excitation levels as seen in Fig. 12.

The shift in resonance frequency as the increase in the excitation levels for the three BLTs is shown in Fig. 14. Results show that the cascaded BLT in L3 mode and the small BLT in L1 mode exhibit more than three times higher frequency shifts at the highest excitation level than the control BLT (3 kHz compared to 600 Hz). For the small BLT in L1 mode this illustrates a proportionate relationship between frequency shift and resonance frequency, with its frequency being three times that of the control BLT. The results are also consistent with the study of control BLTs in Fig. 9 where the PZT to metal ratio is the dominating influence in the nonlinear response. The cascaded and small BLTs show a very close agreement for the frequency shift at increasing displacement amplitude.

The frequency shifts further illustrate the challenges of designing small BLTs as the driver for ultrasonic devices. The next step is to incorporate a gain profile into the front mass of small BLTs to investigate if this mitigates or exacerbates these issues associated with nonlinear dynamic responses.

C. Small Gain-Profile BLTs

A simple approach for miniaturizing an ultrasonic device is to configure the whole device into one half-wavelength of the L1 mode frequency. This means that an amplitude gain profile can be incorporated into the front mass of the BLT. The six small BLTs with different gain profiles are given in Table I. The measured impedance is shown in Fig. 15, which also highlights the differences in resonance frequency for BLTs of a similar length but different front mass profile. All small BLTs were originally tuned to the L1 mode at 45 kHz. However, for example, a slightly shorter prestress bolt was used for the conical shape transducer due to a shallower threaded hole in the front mass. This has resulted in a higher resonance frequency, demonstrating the sensitivity of resonance frequency

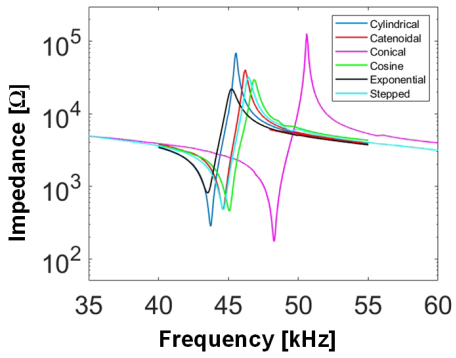

Fig. 15. Measured impedance of the gain-profile BLTs.

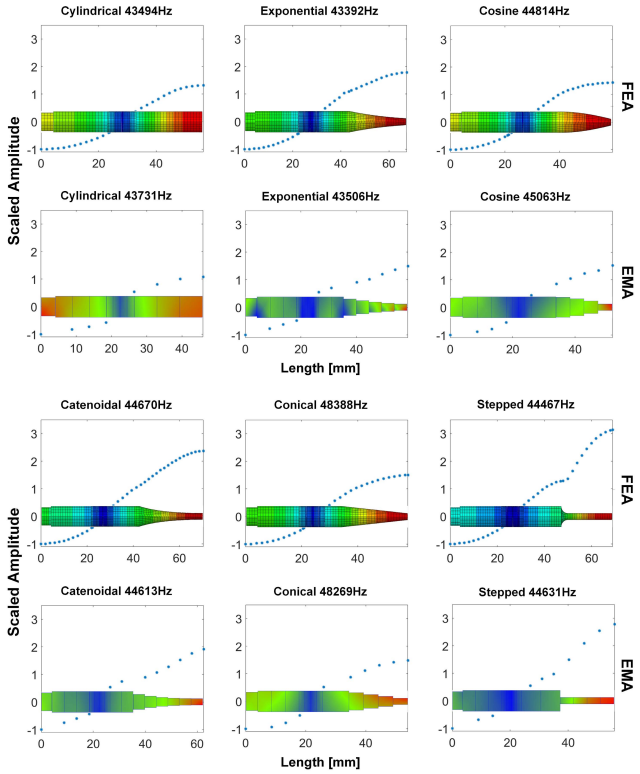

Fig. 16. L1 mode frequencies and mode shapes showing the amplitude gain of the six gain-profile BLTs.

on small differences in mass of metal in the device. The resulting mode shapes and amplitude gains are presented in Fig. 16, demonstrating that the EMA measurements of the BLTs are in close agreement with the predictions performed in the design process using FEA.

The harmonic response analysis results are presented in Fig. 17 and are arranged in ascending order of the maximum displacement amplitude at 100-V excitation level, measured from the front face of the front mass. The measurements are all then summarized in Fig. 18, with the Q estimated from all three measurement methods, and Fig. 19 which presents the resonance frequency shifts at increasing excitation level.

All small BLTs exhibit strong nonlinear responses as expected from the previous studies of the control and cascaded BLTs and this is not mitigated by the addition of a gain profile. However, the achievable amplitude is increased, with the stepped profile BLT achieving close to the target displacement amplitude of 30-μm peak–peak at a 100-V excitation level.

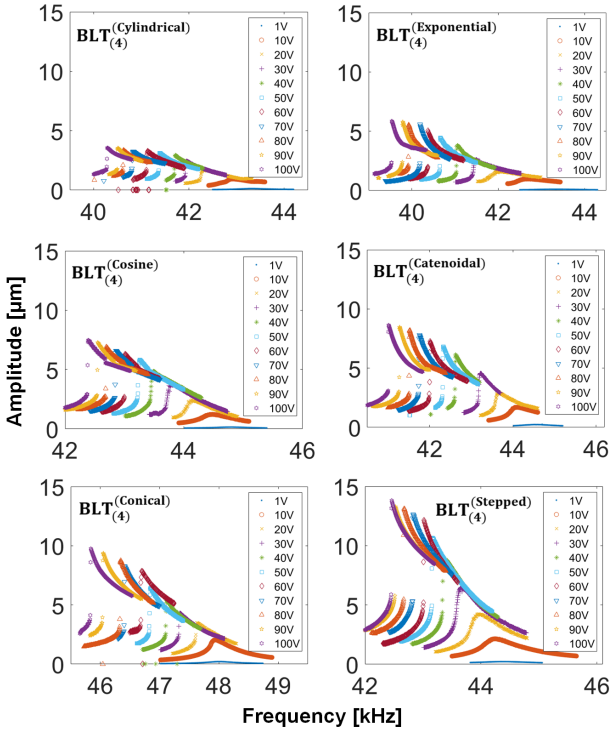

Fig. 17. Vibration response of the gain-profile BLTs at increasing excitation level.

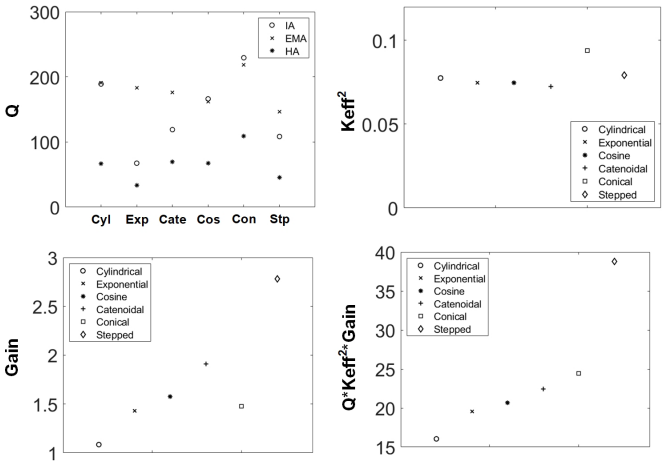

Fig. 18. Q, k_{eff}^2, gain, and ($Q \times k_{\text{eff}}^2 \times$ gain) of the gain-profile BLTs.

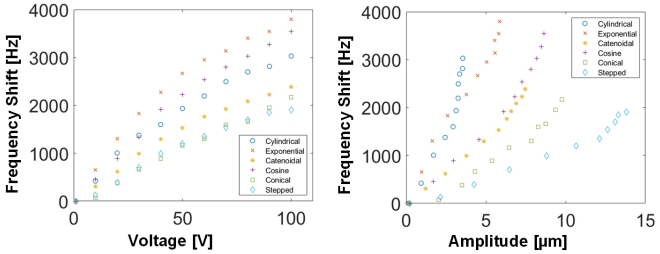

Fig. 19. Resonance frequency shift of gain-profile BLTs at increasing excitation levels and displacement amplitudes.

A significant spread of Q estimations, from around 40 to over 200, is again shown in Fig. 18, with the values estimated from harmonic response analysis being consistently lower than the other two estimations. Both sets of Q estimations from the dynamic characterizations show some consistency across the six BLTs, although the values are very different,

whereas the estimations from impedance measurements vary significantly between BLTs.

k_{eff}^2 values also exhibit only small variations across the BLTs, ranging from 0.07 to 0.09, showing that front mass profile has little effect on the electromechanical coupling. The BLT with a conical front mass has the highest value and this reflects its distinctive, larger bandwidth impedance, as shown in Fig. 15.

The amplitude gain has values from 1.1 (cylindrical) to 2.8 (stepped), as shown in Fig. 16. The order of these gains and the achievable gain for the six geometries diverge from those calculated for large 20-kHz ultrasonic horns reported in a previous study, where the horns were a half wavelength of the L1 mode frequency [40]. In that study, the comparable (i.e., using the same horn base and tip diameter) order and predicted gain values were 10.2 (stepped), 4.1 (cosine), 3.6 (catenoidal), 3.0 (exponential), and 2.4 (conical). This illustrates that theoretical models that are applicable to the large 20-kHz BLTs and gain horns that are widely applied in processes, such as vibration assisted drilling [41], do not scale down well to much smaller and higher frequency devices, especially where the horn is the front mass of the BLT. Fig. 16 shows that the waveforms exhibit a steeper gradient at locations where there are changes in the cross section of the front mass. For large horns, these locations are usually close to a nodal plane and this distinction for small devices significantly affects the gain values.

The resonance frequency shifts (Fig. 19) of the gain-profile BLTs are large, around 4 kHz at 100 V, with the cylindrical profile BLT exhibiting frequency shifts comparable to the cascaded and small BLTs characterized earlier. The data plotted against displacement amplitude show clearly that the BLTs achieving higher amplitudes exhibit smaller frequency shifts, less than 2 kHz, for the conical and stepped profile BLTs, which is important for the control and frequency tracking of small ultrasonic devices.

The proposed figure of merit, $(Q \times k_{\text{eff}}^2 \times \text{gain})$, as shown in Fig. 18, is now dominated by the gain value, but achieves a correction that results in the order of the BLT gain profiles being consistent with the achieved displacement amplitudes in Fig. 17. For devices with similar coupling coefficients, the dynamic response, and therefore achievable amplitude, is affected by the transducer damping as well as the gain profile. As has been indicated in this study, damping is difficult to estimate accurately and therefore a consistent methodology for high power ultrasonic transducers based on dynamic measurements of Q is needed. Interestingly, it is not possible to translate the figure of merit of $(Q \times k_{\text{eff}}^2)$, proposed in a previous study [35], to these gain-profile BLTs as this would result in the conical profile BLT having by far the highest value. It is clear that figures of merit are applicable to a single class of BLTs only and are not useful for configurations that diverge, even slightly, from that class.

Unsurprisingly, the stepped gain profile of the front mass is the most promising design for a small ultrasonic device, achieving the highest displacement amplitude and smallest resonance frequency shift, and this study has shown that it is possible to deliver a small BLT with potential for incorporating in an ultrasonic device, with a size that is consistent with minimally invasive surgeries.

V. Conclusion

A study of different configurations of BLTs is presented with the aim of understanding the limitations and opportunities of designing ultrasonic surgical devices capable of minimally invasive surgeries. Important insights are provided, especially into the trade-offs between the transducer size, volume of piezoceramic material, resonance frequency, and achievable vibration amplitude. Several of these transducer configurations will now be integrated with tips and tested *in vitro* in tissue mimics and animal tissue. It is appreciated that incorporating a surgical tip in the front mass will alter the dynamic response of the device, including the resonance frequency and nonlinear response, but integrating a surgical tip also offers an opportunity to further enhance the gain of the device. The understanding of small BLTs gained in this study will assist in the design of these devices.

Experimental characterizations of a set of control BLTs show that a larger number of piezoceramic rings develop higher electromechanical coupling coefficient, evaluated as k_{eff}^2, however, Q is lower due to the higher number of interfaces and higher PZT to metal ratio. A larger number of PZT rings also lead to a larger resonance frequency shift for increasing excitation levels. It is also shown that for cylindrical BLTs the amplitude gain is not unity, due to the nonuniform mass distribution, which calls into question figures of merit that neglect gain. It is also shown that a more realistic assessment of Q for BLTs is estimated from dynamic measurements rather than transducer impedance measurements. A new figure of merit, $(Q \times k_{\text{eff}}^2 \times \text{gain})$, with Q estimated from EMA is therefore proposed.

The dynamic response is compared of two nominally 20-kHz L1 mode BLTs: one a control and another a cascaded configuration, excited in their L3 modes. These are then compared with a BLT of a third of the length excited in its L1 mode. This illustrates the significant difficulty of exciting sufficient ultrasonic amplitude to cut hard or soft tissues with higher frequency BLTs, with all three BLTs achieving the same displacement amplitude for the excitation levels tested. The results also show that much higher resonance frequency shifts are exhibited at increasing excitation levels, both for the small BLT in L1 mode and the longer cascaded BLT in L3 mode, all excited at a comparable resonance frequency. Interestingly, it is found that the cascaded BLT in L3 mode is a remarkably close proxy for the small L1 mode BLT, both exhibiting very similar dynamic characteristics.

Six BLTs with a gain profile incorporated into the front mass are characterized and the target ultrasonic amplitude of 30-μm peak–peak is achieved for the stepped profile. It is also shown that the order of achievable amplitude of these six BLTs does not match with the theoretical calculations or other figures of merit in the literature. The proposed figure of merit, $(Q \times k_{\text{eff}}^2 \times \text{gain})$, proved to align effectively with the order of achievable displacement amplitude of the BLTs, providing a correction where gain is not the single dominating factor.

A key further issue for future research is that standard characterizations of BLTs provide parameters that are not constant across the excitation levels associated with high power ultrasonic devices. It is shown here that a dynamic estimation of Q is more representative of a BLT under excitation and that resonance frequency can shift significantly for small BLTs, but damping, electromechanical coupling and gain are also excitation-level dependent and this dependence is worthy of further investigation. On a practical level, this affects how impedance matching can be used effectively, with intelligent matching required to enable a better control.

REFERENCES

[1] D. Broughton, A. Welling, E. Monroe, K. Pirozzi, J. Schulte, and J. Clymer, "Tissue effects in vessel sealing and transection from an ultrasonic device with more intelligent control of energy delivery," *Med. Devices: Evidence Res.*, vol. 6, pp. 151–154, Sep. 2013.

[2] G. L. Magrin, E. A. Sigua-Rodriguez, D. R. Goulart, and L. Asprino, "Piezosurgery in bone augmentation procedures previous to dental implant surgery: A review of the literature," *Open Dentistry J.*, vol. 9, no. 1, pp. 426–430, Dec. 2015.

[3] M. Catuna, "Sonic energy: A possible dental application," *Ann. Dentistry*, vol. 12, pp. 100–101, 1953.

[4] T. Vercellotti, S. De Paoli, and M. Nevins, "The piezoelectric bony window osteotomy and sinus membrane elevation: Introduction of a new technique for simplification of the sinus augmentation procedure," *Int. J. Periodontics Restorative Dentistry*, vol. 21, no. 6, pp. 561–567, 2001.

[5] M. Labanca, F. Azzola, R. Vinci, and L. F. Rodella, "Piezoelectric surgery: Twenty years of use," *Brit. J. Oral Maxillofacial Surg.*, vol. 46, no. 4, pp. 265–269, Jun. 2008.

[6] E. Agarwal, S. Masamatti, and A. Kumar, "Escalating role of piezosurgery in dental therapeutics," *J. Clin. Diagnostic Res.*, vol. 8, no. 10, pp. ZE08–ZE11, 2014.

[7] S. Stübinger, A. Stricker, and B. Berg, "Piezosurgery in implant dentistry," *Clin., Cosmetic Investigational Dentistry*, vol. 7, pp. 115–124, Nov. 2015.

[8] A. Franzini *et al.*, "Piezoelectric surgery for dorsal spine," *World Neurosurg.*, vol. 114, pp. 58–62, Jun. 2018.

[9] F. M. Duerr, H. B. Seim, A. L. Bascuñán, R. H. Palmer, and J. Easley, "Piezoelectric surgery—A novel technique for laminectomy," *J. Investigative Surg.*, vol. 28, no. 2, pp. 103–108, Mar. 2015.

[10] P. Leclercq, C. Zenati, S. Amr, and D. M. Dohan, "Ultrasonic bone cut part 1: State-of-the-art technologies and common applications," *J. Oral Maxillofacial Surg.*, vol. 66, no. 1, pp. 177–182, Jan. 2008.

[11] B. J. O'Daly, E. Morris, G. P. Gavin, J. M. O'Byrne, and G. B. McGuinness, "High-power low-frequency ultrasound: A review of tissue dissection and ablation in medicine and surgery," *J. Mater. Process. Technol.*, vol. 200, nos. 1–3, pp. 38–58, May 2008.

[12] K. Ebina, H. Hasegawa, and H. Kanai, "Investigation of frequency characteristics in cutting of soft tissue using prototype ultrasonic knives," *Jpn. J. Appl. Phys.*, vol. 46, no. 7B, pp. 4793–4800, Jul. 2007.

[13] D. G. Nicastri, M. Wu, J. Yun, and S. J. Swanson, "Evaluation of efficacy of an ultrasonic scalpel for pulmonary vascular ligation in an animal model," *J. Thoracic Cardiovascular Surg.*, vol. 134, no. 1, pp. 160–164, Jul. 2007.

[14] R. Cox, "Getting the most out of ultrasonic scaling: A guide to maximizing efficacy," *Acad. General Dentistry*, pp. 1–6, 2015.

[15] G. Plotino, C. Pameijer, N. Mariagrande, and F. Somma, "Ultrasonics in endodontics: A review of the literature," *J. Endodontics*, vol. 33, no. 2, pp. 81–95, Feb. 2007.

[16] J. Yang, Q. Zhang, and T. Xu, "A novel piezoelectric ceramic actuator with scissoring composite vibration for medical applications," *Appl. Sci.*, vol. 9, no. 21, p. 4637, Oct. 2019.

[17] S. C. Lea, B. Felver, G. Landini, and A. D. Walmsley, "Three-dimensional analyses of ultrasonic scaler oscillations," *J. Clin. Periodontol.*, vol. 36, no. 1, pp. 44–50, Jan. 2009.

[18] M. Schafer, "Ultrasonic surgical devices and procedures," in *Power Ultrasonics*. Cambridge, U.K.: Woodhead, 2015.

[19] Y. Kuang, Y. Jin, S. Cochran, and Z. Huang, "Resonance tracking and vibration stablilization for high power ultrasonic transducers," *Ultrasonics*, vol. 54, no. 1, pp. 187–194, Jan. 2014.

[20] F. Bejarano, A. Feeney, R. Wallace, H. Simpson, and M. Lucas, "An ultrasonic orthopaedic surgical device based on a cymbal transducer," *Ultrasonics*, vol. 72, pp. 24–33, Dec. 2016.

[21] N. Simaan, R. M. Yasin, and L. Wang, "Medical technologies and challenges of robot-assisted minimally invasive intervention and diagnostics," *Annu. Rev. Control, Robot., Auto. Syst.*, vol. 1, no. 1, pp. 465–490, May 2018.

[22] A. Orekhov, C. Abah, and N. Simaan, "Snake-like robots for minimally invasive, single-port, and intraluminal surgeries," in *The Encyclopedia of Medical Robotics*, vol. 1. 2018, pp. 203–243.

[23] M. Runciman, A. Darzi, and G. P. Mylonas, "Soft robotics in minimally invasive surgery," *Soft Robot.*, vol. 6, no. 4, pp. 423–443, Aug. 2019.

[24] H. Kharosekar, S. Jasmit, S. Valsangkar, D. Palande, and V. Velho, "Ultrasonic osteotome: A cutting edge technology, our experience in 96 patients," *Indian J. Neurosurg.*, vol. 3, no. 3, pp. 150–153, Jan. 2017.

[25] S. C. Lea, G. Landini, and A. D. Walmsley, "Displacement amplitude of ultrasonic scaler inserts," *J. Clin. Periodontol.*, vol. 30, no. 6, pp. 505–510, Jun. 2003.

[26] S. C. Lea, G. Landini, and A. D. Walmsley, "The effect of wear on ultrasonic scaler tip displacement amplitude," *J. Clin. Periodontol.*, vol. 33, no. 1, pp. 37–41, Jan. 2006.

[27] K. Desinger, K. Liebold, J. Helfmann, T. Stein, and G. Müller, "A new system for a combined laser and ultrasound application in neurosurgery," *Neurological Res.*, vol. 21, no. 1, pp. 84–88, Jan. 1999.

[28] V. K. Astashev and K. A. Pichygin, "Resonance adjustment and optimization of parameters of an ultrasonic rod system with a piezoelectric vibration exciter," *J. Machinery Manuf. Rel.*, vol. 42, no. 5, pp. 347–352, Sep. 2013.

[29] V. K. Astashev, K. A. Pichugin, X. Li, A. Meadows, and V. I. Babitsky, "Resonant tuning of langevin transducers for ultrasonically assisted machining applications," *IEEE Trans. Ultrason., Ferroelectr., Freq. Control*, vol. 67, no. 9, pp. 1888–1896, Sep. 2020.

[30] J. Kim and J. Lee, "Parametric study of bolt clamping effect on resonance characteristics of Langevin transducers with lumped circuit models," *Sensors*, vol. 20, no. 7, pp. 1–9, 2020.

[31] C.-H. Choi *et al.*, "Relation between piezoelectric properties of ceramics and output power density of energy harvester," *J. Eur. Ceram. Soc.*, vol. 33, no. 7, pp. 1343–1347, Jul. 2013.

[32] F. J. Arnold and S. S. Mühlen, "The mechanical pre-stressing in ultrasonic piezotransducers," *Ultrasonics*, vol. 39, no. 1, pp. 7–11, Jan. 2001.

[33] A. Caronti, R. Carotenuto, and M. Pappalardo, "Electromechanical coupling factor of capacitive micromachined ultrasonic transducers," *J. Acoust. Soc. Amer.*, vol. 113, no. 1, pp. 279–288, Jan. 2003.

[34] S. Zhang and T. R. Shrout, "Relaxor-PT single crystals: Observations and developments," *IEEE Trans. Ultrason., Ferroelectr., Freq. Control*, vol. 57, no. 10, pp. 2138–2146, Oct. 2010.

[35] T. Hemsel, E. G. Lierke, W. Littmann, and T. Morita, "Various aspects of the placement of a piezoelectric material in composite actuators, motors, and transducers," *J. Korean Phys. Soc.*, vol. 57, no. 4, pp. 933–937, Oct. 2010.

[36] P. Avitabile, "Experimental modal analysis," *Sound Vib. Mag.*, vol. 35, no. 1, pp. 1–15, 2001.

[37] M. Garcia-Rodriguez *et al.*, "Low cost matching network for ultrasonic transducers," *Phys. Procedia*, vol. 3, no. 1, pp. 1025–1031, Jan. 2010.

[38] A. Mathieson, A. Cardoni, N. Cerisola, and M. Lucas, "Understanding nonlinear vibration behaviours in high-power ultrasonic surgical devices," *Proc. Roy. Soc. A, Math., Phys. Eng. Sci.*, vol. 471, no. 2176, Apr. 2015, Art. no. 20140906.

[39] A. Albareda, R. Pérez, J. Casals, J. García, and D. Ochoa, "Optimization of elastic nonlinear behavior measurements of ceramic piezoelectric resonators with burst excitation," *IEEE Trans. Ultrason., Ferroelectr., Freq. Control*, vol. 54, no. 10, pp. 2175–2188, Oct. 2007.

[40] V. Astashev and V. Babitsky, "Ultrasonic processes and machines," in *Dynamics, Control and Applications*. Berlin, Germany: Springer-Verlag, 2007.

[41] S. Addepalli, "Modal analysis of horns used in ultrasonic vibration assisted drilling," *Int. J. Innov. Eng. Technol.*, pp. 294–298, 2016.